Pseudoelastic Behavior of a CuAlNi Single Crystal under Uniaxial Loading

DAI-NING FANG, WEI LU, and KEH-CHIH HWANG

In order to study the basic properties of pseudoelasticity of a CuAlNi single crystal, an investigation was carried out to observe and analyze the orientation dependence of the stress-induced martensitic transformation. The transformation is the β_1 to β_1' stress-induced transformation in a Cu-13.7 pct Al-4.18 pct Ni (wt pct) alloy. From the uniaxial tension of three groups of differently oriented flat specimens, we obtained a series of stress-strain curves. In addition, the micrograph of martensitic evolution was observed by utilizing a long-focus microscope. It is found that martensite appears in the shape of bands or thin plates on the surface of the specimen. The formation of martensite is a very quick process, and martensite "jumps" out until the specimen is completely transformed into a single variant. The experimental results are analyzed and compared to a constitutive model proposed recently. It is found that the constitutive model cannot describe transformation hardening, since the model ignores the surface-energy change. Nevertheless, the proposed constitutive model cannot only precisely predict the forward and reverse transformation, but can also characterize the stress-strain hysteresis behavior during pseudoelastic deformation under uniaxial tension loading.

I. INTRODUCTION

STRESS-induced martensitic transformations have been studied in a number of alloys.[1–10] An important characteristic of shape-memory alloys (SMAs) is the ability to undergo a diffusionless, structural, and reversible martensitic phase transformation. The martensitic transformation is accompanied by a large shear-like deformation, which generally amounts to about 20 times more than the elastic deformation. The martensite may be induced from the parent phase either by loading or by cooling. Detailed investigations on thermoelastic martensitic transformation have been done in the fields of physics and materials science. A quite complete theoretical system, which includes the transformation crystallographic theory, thermodynamics, *etc.*, has been established by Wechsler *et al.*,[1] Wayman,[2] Bowles and Mackenzie,[3] Delaey *et al.*,[4] Christian,[5] James,[6] Ball and James,[7] Bhattacharya,[8] Abeyaratne *et al.*,[9,10] and many others. On the other hand, with the increasing application of SMAs and structural ceramics, the study on the constitutive relation of the materials with thermoelastic martensitic transformation attracts the interest of researchers of solid mechanics. For example, much work has been done by Falk,[11] Patoor *et al.*,[12] Abeyaratne *et al.*, Muller and Xu,[13] Chu and James,[14] Tanaka *et al.*,[15,16] Liang and Rogers,[17] Sun and Hwang,[18,19] Fischer *et al.*,[20,21] Yan *et al.*,[22,23,24] Chen *et al.*,[25] Song *et al.*,[26] Lu and Weng,[27] and many others. The pseudoelastic phenomena of SMA single crystals under uniaxial loading have been investigated by authors such as Okamoto *et al.*,[28] Horikawa *et al.*,[29] Shield,[30] and many others.

It is generally believed that the shape strain defined by an invariant plane strain along a habit plane interacts with an applied stress, and, thus, a habit plane is selected by a maximum Schmid factor for the shape strain.[30,31,32] In a series of articles, Ichinose, Otsuka, and Horikawa *et al.*[29,33] reported their research results of pseudoelastic phenomena of CuAlNi single crystals under uniaxial loading. Suezawa and Sumino[34] obtained the theoretical expression of the relation between the elastic constants of a CuAlNi single crystal and its orientations. However, there still remain some important problems regarding the orientation dependence. These include the selection of a habit plane variant under stress, the orientation dependence of transformation stress and strain, *etc.* For example, a systematic observation and recording of the microstructural changes during loading and unloading has always been a difficult problem which hampers us from a clear understanding of the process. The orientation dependence of critical stress is also an interesting subject. The purpose of the present article is to provide reliable experimental data on the orientation dependence of the β_1 to β_1' stress-induced transformation in a CuAlNi alloy and the microstructural changes at different stress-strain states.

CuAlNi alloys near the composition Cu-14 pct Al-4 pct Ni (wt pct) transform from the β_1 parent phase (DO_3-type ordered structure) to the γ_1' martensitic phase (2H-type stacking-order structure in Ramsdel notation) upon cooling.[34–37] However, when a stress is applied, the γ_1' martensite is stress induced at temperatures near the M_s point, while the β_1' martensite (18R-type long-period stacking-order structure) is stress induced at temperatures roughly above the A_f point.[37,38,39] This is the stress-induced transformation from β_1 to β_1', which was observed in this investigation. The β_1' martensite appears as a stack of thin plates, and the transformation is characterized by a smooth stress-strain curve and by a very small stress hysteresis.[37] By using the parameters given in Reference [37], we obtained the habit planes and transformations for the 24 variants in terms of Wechsler-Lieberman-Read (WLR) theory,[1,2] and the calculated results from WLR theory are compared to the observed data from the experiments.

DAI-NING FANG and KEH-CHIH HWANG, Professors, and WEI LU, Research Assistant, are with the Department of Engineering Mechanics, Tsinghua University, Beijing 100084, P.R. China.

Manuscript submitted August 6, 1998.

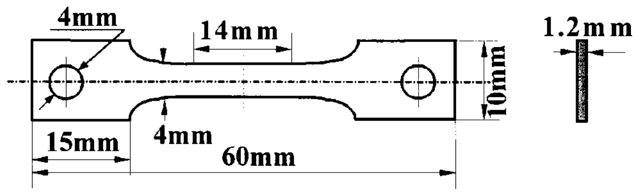

Fig. 1—The geometry and dimension of the tensile specimen.

Table I. Loading Directions and Normal Directions of the Surface of the Three Groups of Specimens

Group Number of Specimen	Loading Direction, t	Normal Direction of Specimen Surface, n^s
S1	(0.027, 0.381, 0.924)	(0.731, 0.623, −0.278)
S2	(0.917, −0.174, −0.358)	(0.375, 0.075, 0.924)
S3	(0.717, −0.696, −0.046)	(0.076, 0.012, 0.997)

Yan *et al.*[22,23,24] established a generalized micromechanics-constitutive theory to describe the thermoelastic martensitic forward transformation, reverse transformation, and reorientation of single crystals induced by applied stress and/or temperature. The transformation plastic strain is obtained from the crystallographic theory for martensitic transformation directly. The free energy of the constitutive element is derived by means of micromechanics approaches. The volume fractions of various kinds of martensite variants are considered as internal variables which describe the pattern of internal rearrangement resulting from the phase transformation and reorientation in the loading history. In the framework of the Hill–Rice internal-variable thermodynamics-constitutive theory, the forward transformation, reverse transformation, reorientation yield functions, and incremental stress-strain relations are formulated. We will briefly introduce Yan's work in this article, for the purpose of comparing his theory to the experimental data.

The rest of this article is as follows. Section II introduces the uniaxial tensile setup and the experimental procedure. The experimental results are presented in Section III. In Section IV, the results of the orientations and transformation plastic strain of 24 martensite variants, calculated by means of the crystallographic theory for martensitic transformation, are presented and compared to experimental results. For completeness of the article, in Section V, the proposed micromechanics-constitutive model is briefly introduced, and then the comparison of the theoretical predictions to experimental data is made. The conclusions are given in Section VI.

II. EXPERIMENTAL PROCEDURE

The Cu-13.7 pct Al-4.18 pct Ni (wt pct) single crystal was grown by the modified Bridgman method.[40] An as-grown crystal having the shape of a cylinder, with a diameter of 22 mm and length of 65 mm, was obtained. Flat tensile specimens with pin-loaded ends were made by means of cutting the cylindrical crystal along its longitudinal axis. Figure 1 gives the geometry and dimension of the tensile specimens. The specimens were first heated to 850 °C and kept at this temperature for 5 minutes, then they were drenched in a solution of 10 pct NaOH at room temperature (26.5 °C) for 30 minutes. The transformation temperatures were determined by differential scanning calorimetry (DSC) and are $M_s = -20$ °C, $M_f = -49$ °C, $A_s = -19$ °C, and $A_f = 0$ °C. Therefore, the specimen is austenitic at room temperature. The orientations of the single-crystal specimen were obtained by X-ray back-reflection Laue methods. The orientations of the three groups of the flat specimens used in the experiments are expressed in the coordinates of the parent phase, as listed in Table I. Each specimen was precisely polished on one side in order to observe, by use of a

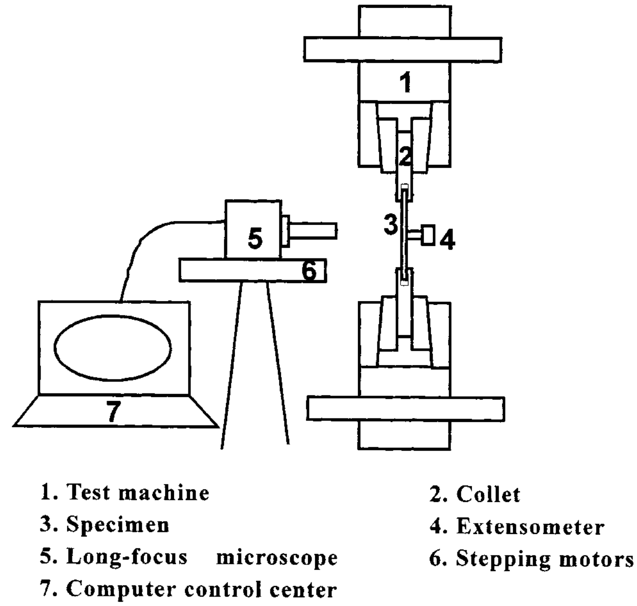

Fig. 2—Schematic of the experimental setup.

long-focus microscope, the microstructural changes on the surface during loading and unloading. The typical morphological changes, such as the appearance of martensitic stripes, their geometrical shape, and distribution, were observed. Although we tried our best to polish the specimens, which were polished along the loading axis, there still exist some longitudinal scratches on the surface because the Cu-based alloy is quite soft. In addition, a newly polished surface usually oxidizes after 6 hours and then turns gray. Therefore, in our experiments, a specimen was tested within 2 hours after its polishing. To the other side of the specimen, which was not polished, was attached a miniature extensometer that can measure strain as large as 10 pct. The schematic of the experimental setup is shown in Figure 2. The main components in the setup include the (1) test machine, (2) collet, (3) specimen, (4) extensometer, (5) long-locus microscope, (6) stepping motors, and (7) computer-control stage. Tension along the longitudinal axis of the flat specimen was applied by a SHIMADZU test machine. Stress signals from the load cell and strain signals from the extensometer were transmitted to a recorder. A computer controls the stepping motors that drive a stage on which the long-focus microscope is mounted, so that the long-focus microscope can move precisely with the tension direction. In this way, we could track a selected observation point on the surface of the specimen. In order to minimize the undesired external effects, light is transmitted by a special light fiber and is

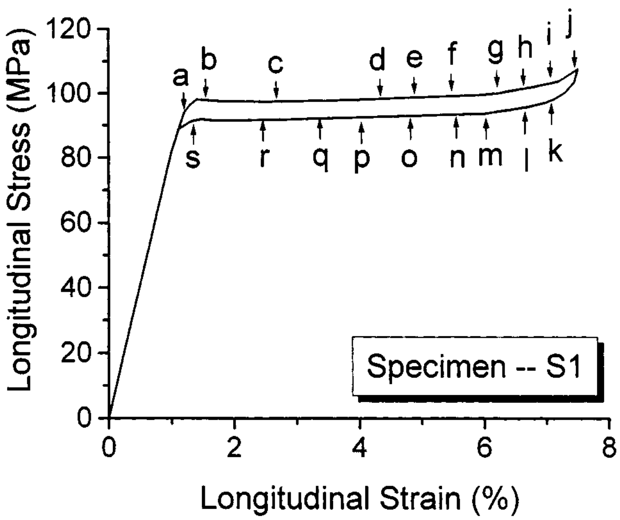

Fig. 3—Measured stress-strain curve for specimen S1.

focused on the observation point. A close-coupled device camera is mounted on the long-focus microscope, so that the optical micrograph can be shown on the screen of the computer.

III. EXPERIMENTAL RESULTS

Figure 3 shows the stress-strain curves for specimen S1. Typical morphological changes on the surface of the S1 specimen are shown in the series of micrographs in Figures 4(a) through (s), with the corresponding points (a) through (s) marked on the stress-strain curve of Figure 3. Specimens S2 and S3 have similar micrographs. It can be seen from Figure 3 that the stress-strain curve demonstrates obvious pseudoelasticity. In Figure 3, points (a) through (i) correspond to the loading process, and points (k) through (s) correspond to unloading. The material is austenitic when the loading is small, and no phase transformation occurred. The curve is linear in this stage. When the stress reaches the transformation stress, martensite begins to appear. In this article, we define the average stress level in the "plateau" as the transformation stress. The change of the material structure in this stage is from DO_3 (β_1 phase) to 18R (β_1' phase). A clear stress-plateau stage occurs during the phase transformation, because only one kind of variant appears and there is no orientation rearrangement. The same phenomenon can also be observed from the micrographs shown in Figure 4. The martensite bands or thin plates are parallel to each other, which means that only one variant appears. The stress increases slowly during the phase transformation, which indicates that the material still has a slight hardening effect. The further increase of stress from point i to point j causes the specimen to become a complete single crystal of martensite (at least on the optical microscopic scale). Before the applied stress reaches a value below which no permanent plastic deformation is induced, the unloading can be performed, and the stress-strain curve is linear elastic until it reaches the stage of reverse phase transformation again. The stress-plateau stage appears again, and reverse martensitic transformation appears. It can be found that the reverse transformation stress is lower than the forward transformation, which reveals that energy dissipation occurs during the loading and unloading cycle. The stress-strain hysteresis found in the experiment is an important character of the pseudoelastic phenomenon, which distinguishes it from the classic elastic deformation.

The series of micrographs in Figure 4, which correspond to the points marked in Figure 3, illustrate the obvious morphological change associated with the $\beta_1 \Leftrightarrow \beta_1'$ transformation. In order to determine the characteristics given in Figures 4(a) through (s), Figure 4(t) shows the schematic of the micrograph with such information as the loading direction (t), martensite bands, orientation of the martensite variant (u), and the angle (θ) between the martensite band and the loading direction. Martensite appears in the shape of bands or thin plates on the surface of the specimen. Upon loading (points a through i), starting from the β_1 matrix phase, as shown in Figure 4(a), the material is austenitic and the micrograph is gray (Figure 4(a)). No morphological change occurs in the linear elastic range until point b is reached in the stress-strain curve, where a few martensite bands or thin plates appear, as shown in Figure 4(b). That is, when the external stress reaches the transformation stress, martensite bands begin to appear, which are brighter than the austenite (Figure 4(b)). With increasing strain, more and more martensite bands or thin plates are nucleated, and some of them coalesce into thicker plates since only one variant is favored by the Schmid factor. After eventual coalescence at point i, the specimen becomes essentially a single crystal on the microscopic scale, although a few matrix regions are still observable in Figure 4(i). It is observed that the martensite bands are parallel to each other, which means that only one variant appears. It is found in the experiment that the appearance of martensite is a very quick process, and martensite always "jumps" out until the specimen becomes, essentially, a single crystal. Another important phenomenon is that the martensite thin plates are distributed uniformly, which may be due to the fact that, although the occurrence of martensite favors a reduction in the local stress concentration so that the speed of martensite formation slows down or stops, the stress in other parts is still large and the martensite in those regions grows rapidly.

In order to analyze the evolution of martensite in another way, we manipulate the micrographs in Figure 4 by means of an image binary technique to get clearer plots, as shown in Figure 5. That is, the micrographs of Figure 4 can be processed in terms of two colors, such as black and white. The black represents austenite and the white represents martensite. From Figure 5, which just gives some examples of micrographs relative to the loading process, we can precisely obtain the angle between the martensite plates and the loading direction, which is 93.9 deg, as shown in Figures 4(c) and (t) and 5. It must be pointed out from Figure 5 that the coalescence of martensite plates cannot be quantitatively characterized.

IV. MARTENSITE CRYSTALLOGRAPHY

In the proposed micromechanics-constitutive model, the microscopic transformation plastic strain has to be calculated first. By use of the martensitic transformation crystallographic theory developed by Wechsler *et al.*[1] as well as by Bowles and Mackenzie,[2] and in terms of the measured

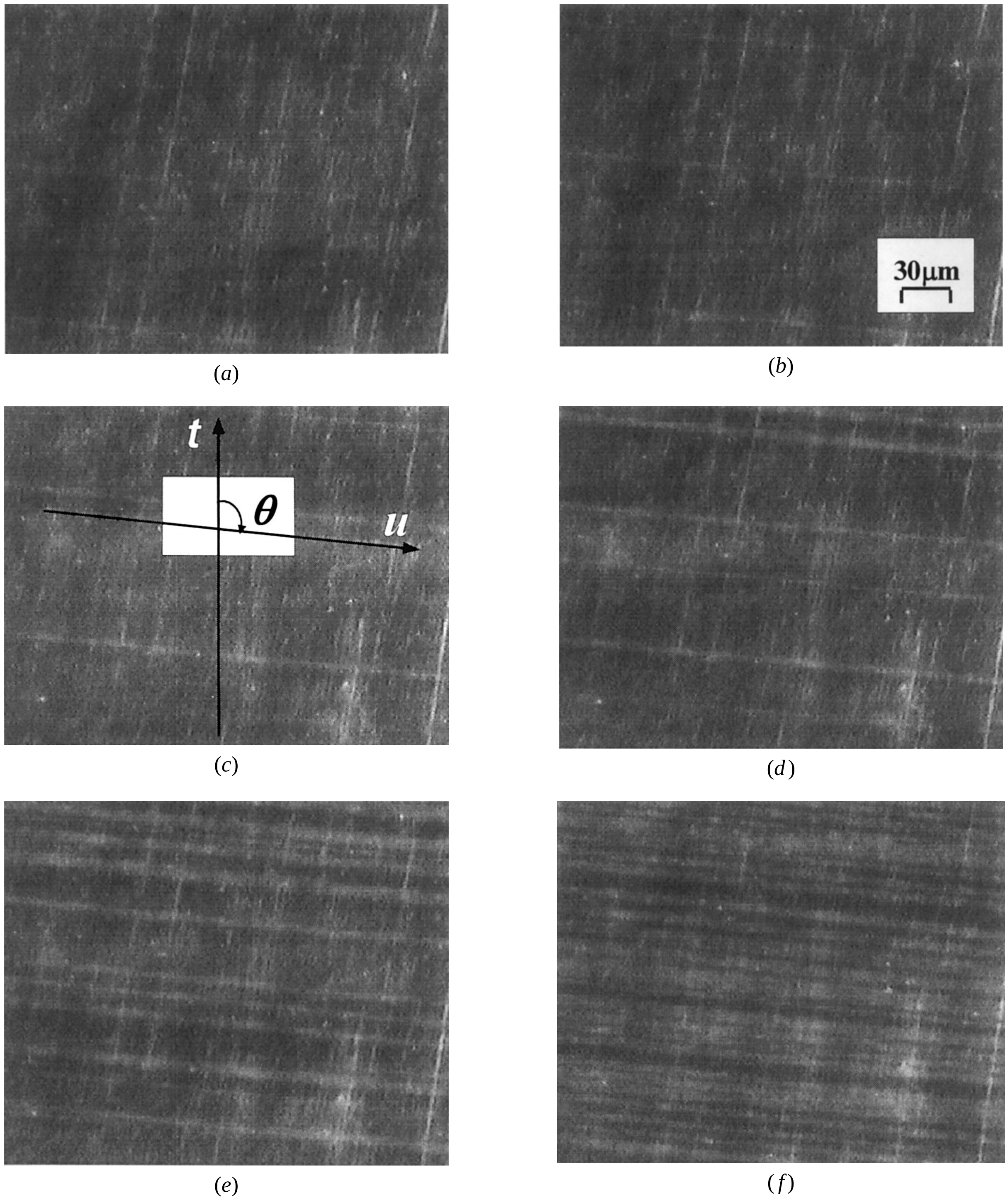

Fig. 4—Microscopic morphological change associated with the stress-induced transformation for specimen S1, (*a*) through (*s*) correspond to the points marked in Fig. 3.

lattice values of the CuAlNi single crystal, the habit planes of the 24 variants and the transformation-induced strain relative to the 24 variants can be predicted. The main content of the crystallographic theory is that martensitic transformation is realized through an invariant plane strain, which is a terminology of materials science and is actually a kind of deformation-gradient tensor in light of continuum mechanics. As shown in Figure 6, the invariant plane strain (*i.e.*, deformation-gradient tensor, **D**) can be expressed by

$$\mathbf{D} = \mathbf{I} + g\mathbf{en} \qquad [1]$$

where **I** is the identity tensor of rank two, **e** is the unit vector displacement direction of the invariant plane, **n** is the unit vector normal to the invariant plane, and g is the displacement magnitude of the invariant plane per unit length along the normal direction (**n**). According to the small deformation theory, the corresponding transformation strain ($\boldsymbol{\varepsilon}^p$) can be easily written as

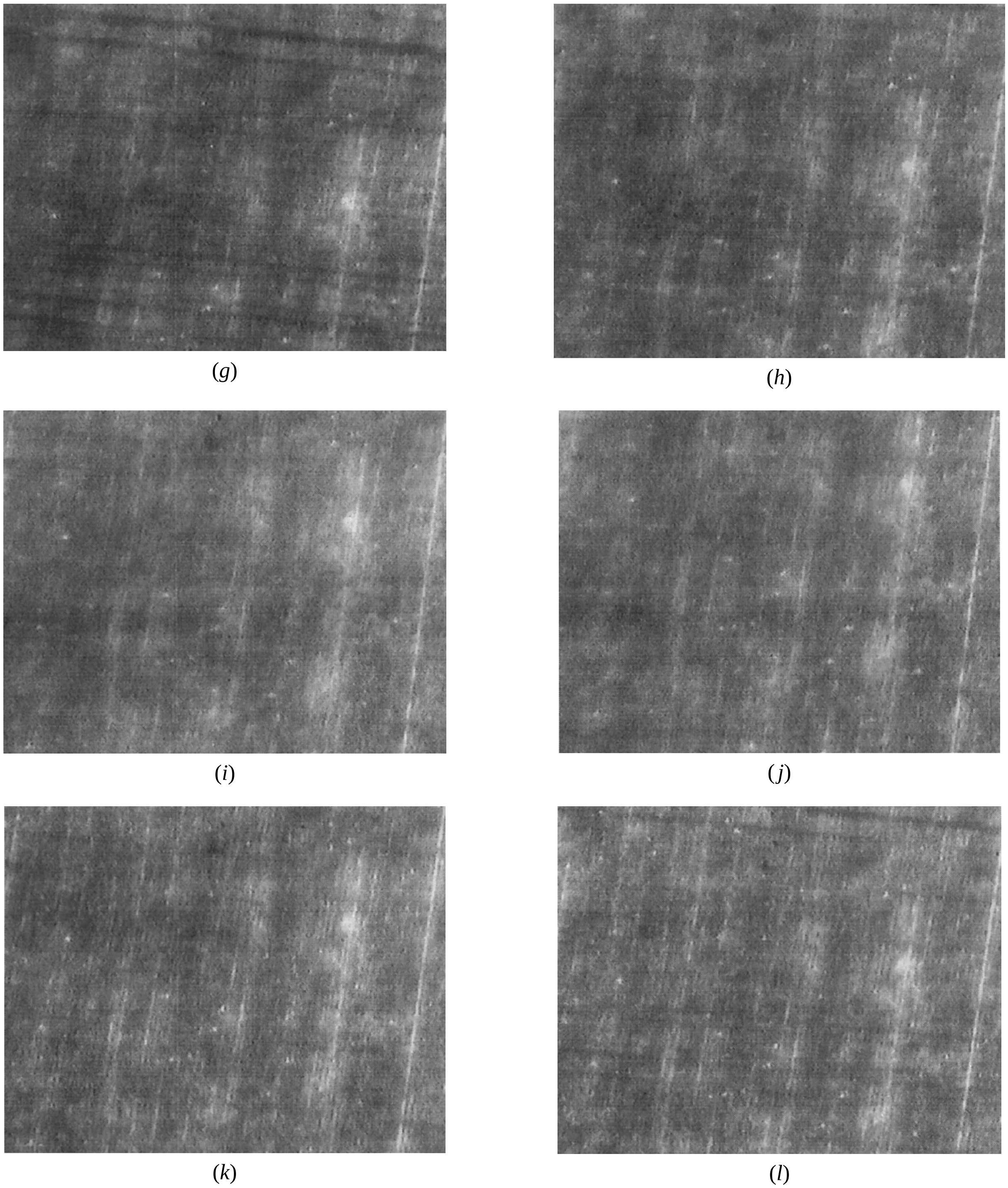

Fig. 4—(continued) Microscopic morphological change associated with the stress-induced transformation for specimen S1, (*a*) through (*s*) correspond to the points marked in Fig. 3.

$$\boldsymbol{\varepsilon}^p = \frac{1}{2} g(\mathbf{en} + \mathbf{ne}) \qquad [2]$$

We define

$$\mathbf{R} = \frac{1}{2} (\mathbf{en} + \mathbf{ne}) \qquad [3]$$

where $\mathbf{R}$ is the orientation tensor of the martensite variant. In terms of the crystallographic theory for martensitic transformation, we can determine all the possible kinds of martensite variants with different orientations. The orientation tensor of the sth kind of variant ($\mathbf{R}_s$), which is crystallographically permissive, can be obtained by Eq. [3]. Thus, we can calculate the microscopic transformation strain corresponding to the sth kind of variant by

$$\boldsymbol{\varepsilon}_s^p = g\mathbf{R}_s = \frac{1}{2} g(\mathbf{e}_s\mathbf{n}_s + \mathbf{n}_s\mathbf{e}_s) \ (s = 1, \ldots, N) \qquad [4]$$

where N is the number of kinds of variants. The parent phase of CuAlNi single crystal has a cubic DO_3 structure and belongs to the β_1 alloy, whose lattice parameter is $a_0 =$

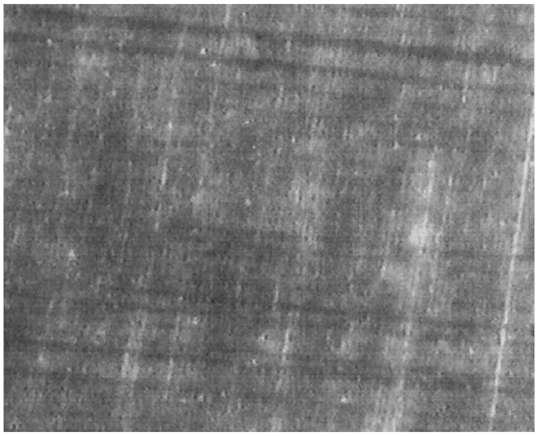

(*m*)

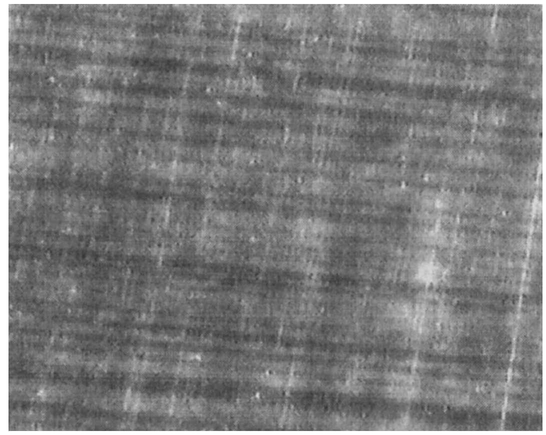

(*n*)

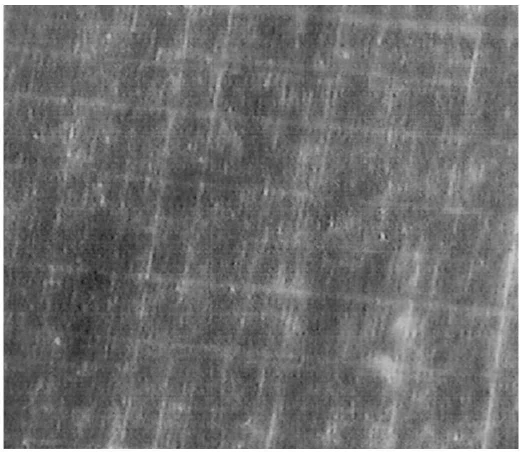

(*o*)

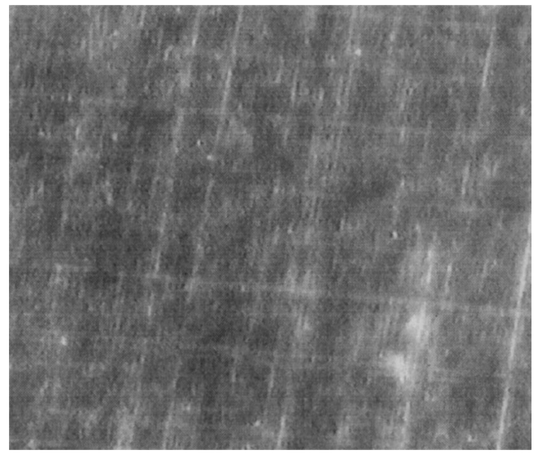

(*p*)

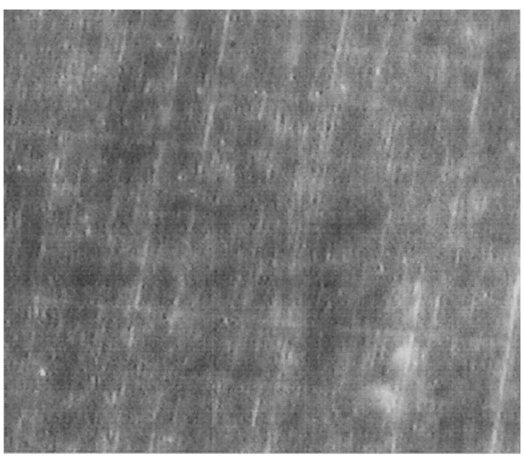

(*q*)

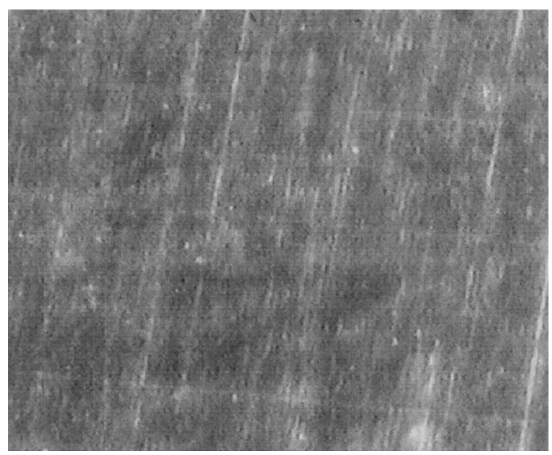

(*r*)

Fig. 4—(continued) Microscopic morphological change associated with the stress-induced transformation for specimen S1, (*a*) through (*s*) correspond to the points marked in Fig. 3.

5.836 Å, while the β_1' martensite has a 18R-type long-period stacking order, with lattice parameters of $a = 4.382$ Å, $b = 5.356$ Å, and $c = 38.00$ Å.[37] In terms of the crystallographic theory and the measured lattice values of the CuAlNi single crystal, the unit vector normal to each invariant plane ($\mathbf{n}_s$) and the unit vector displacement direction of each invariant plane ($\mathbf{e}_s$) are calculated. Substituting the normal and the unit-vector displacement direction of the habit planes of the 24 kinds of variants into Eq. [4], we can get the transformation strains of the 24 kinds of variants expressed in the crystallographic directions of the parent phase as well.

After obtaining the geometry of the 24 variants according to the crystallography theory, we can predict the angle between the martensite plate and the loading direction. Let $\mathbf{n}$ be the normal of the invariant planes, $\mathbf{n}^s$ the normal of the surface of the flat specimen, and t the longitudinal tension

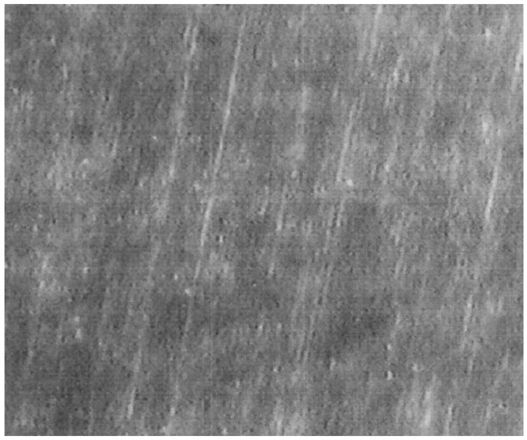

(*s*)

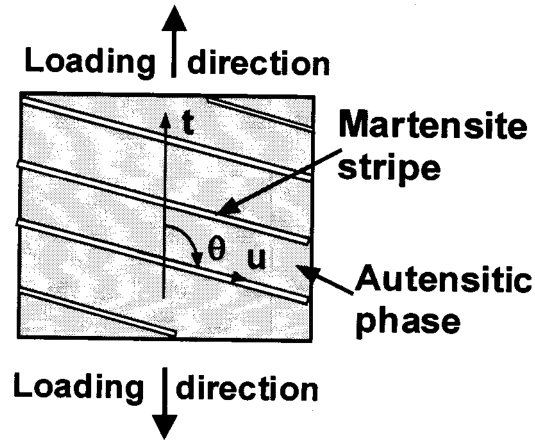

(*t*)

Fig. 4—(continued) Microscopic morphological change associated with the stress-induced transformation for specimen S1, (*a*) through (*s*) correspond to the points marked in Fig. 3.

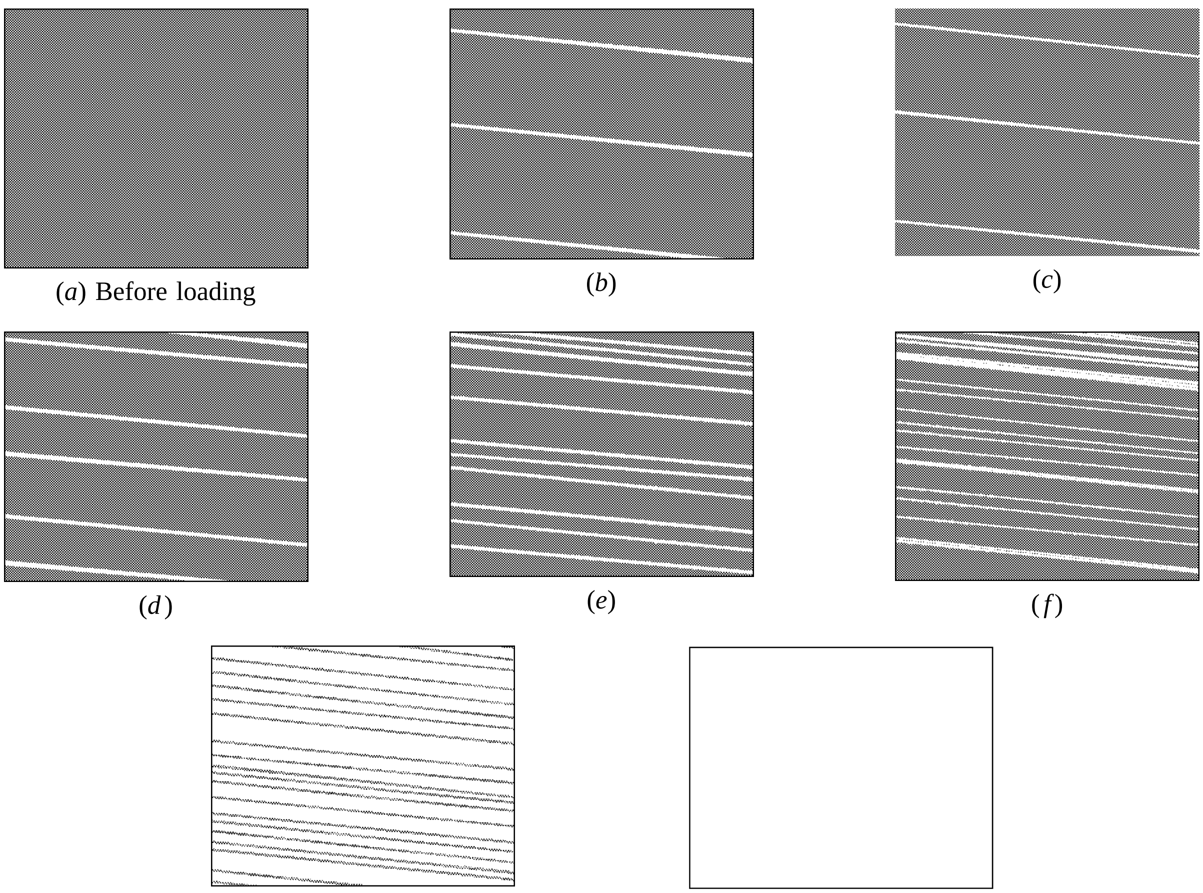

(*a*) Before loading (*b*) (*c*) (*d*) (*e*) (*f*) (*g*) (*j*)

Fig. 5—Micrograph after binarization.

direction of the specimen, as shown in Figure 7. The intersection line between the invariant plane and the surface of the flat specimen, ($\mathbf{u}$), can be expressed by

$$\mathbf{u} = \mathbf{n} \times \mathbf{n}^s \qquad [5]$$

The angle between the invariant plane and the loading direction, can be expressed by

$$\cos\,\theta = \frac{\mathbf{u} \cdot \mathbf{t}}{\sqrt{(\mathbf{u} \cdot \mathbf{u})}\,\sqrt{(\mathbf{t} \cdot \mathbf{t})}} \qquad [6]$$

where θ is defined as the angle from $\mathbf{t}$ to $\mathbf{u}$ in a right-handed direction relative to $-\mathbf{n}^s$. Then,

$$d = (\mathbf{t} \times \mathbf{u}) \cdot \mathbf{n}^s \qquad [7]$$

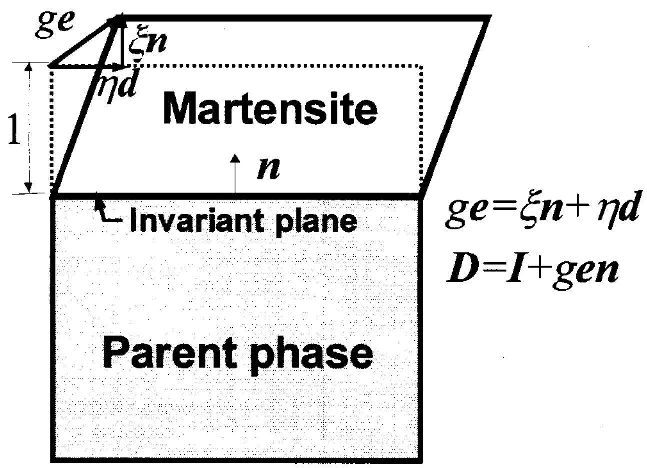

Fig. 6—Illustration of invariant plane deformation.

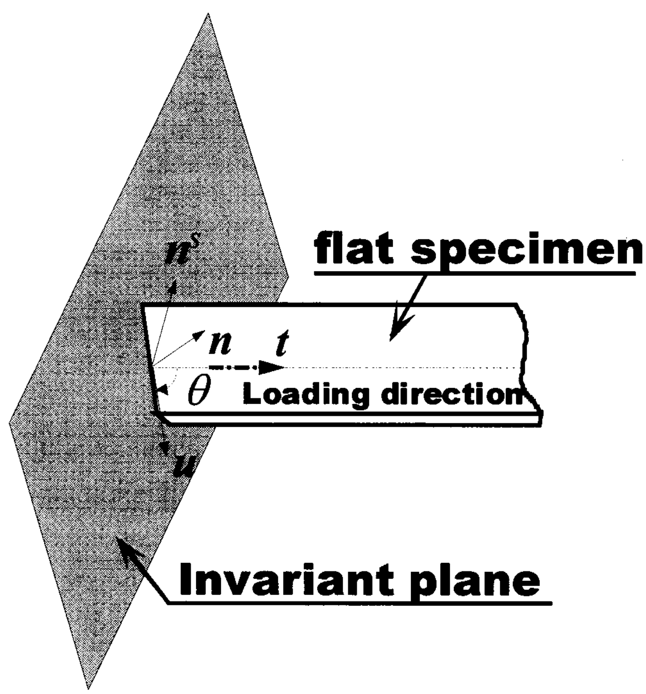

Fig. 7—Schematic of the intersection of invariant planes on the surface of the specimen.

The range of the angle can be determined by the sign of d expressed in Eq. [7]. If $d \leq 0$, then $0 \leq \theta \leq 180$ deg; if $d > 0$, then 180 deg $< \theta <$ 360 deg. As measured from the experiments, the normal of the specimen, is (0.7312, 0.6229, $-$0.2782) and the loading direction is (0.0270, 0.3811, 0.9241). Based on Eqs. [6] and [7], the calculated values of the angles between the intersection lines of the 24 invariant planes on the surface of the specimen and the loading direction are listed in Table II. On the other hand, we can measure the angle between the martensite plates and the loading direction directly from the micrograph of Figure 4. For example, the angle between the martensite plates and the loading direction for specimen S1 is 93.9 deg, which is very close to the calculated angle between the intersection line of the 13th invariant plane on the surface of the specimen and the loading direction. The difference is only 0.8 deg. The measured angles corresponding to the relevant variant number for specimens S1, S2, and S3 are given in Table II, respectively, which indicates that the 13th variant appears in specimen S1, the 24th variant in specimen S2, and the 10th variant in specimen S3. As pointed out in the previous section, during the pseudoelastic transformation induced by the unixial-tension loading at a temperature above A_f, only one variant appears in the process of forward transformation from the parent phase to the martensite phase (*i.e.*, $p \rightarrow m$). This variant disappears in the process of reverse transformation from the martensite phase to the parent phase (*i.e.*, $m \rightarrow p$). Therefore, by measuring the angle of inclination of the martensite plate, we can experimentally determine which variant appears during the pseudoelastic deformation during the unixial-tension loading at a temperature above A_f. For instance, from the results listed in Table II, we can know that the processes of the forward and reverse transformation for specimens S1, S2, and S3 are $p \rightarrow m(13) \rightarrow p$, $p \rightarrow m(24) \rightarrow p$, and $p \rightarrow m(10) \rightarrow p$, respectively. In the next section, the theoretical results obtained from a proposed constitutive model[22,24] show that exactly the same processes of forward and reverse transformation can be predicted for the three types of differently oriented specimens.

V. COMPARISON OF THEORY AND EXPERIMENTS

In this section, our experimental results are compared to the constitutive model proposed by Yan *et al.*[22,23,24] and Song *et al.*[26] Leaving the details to the original articles, the basic assumptions and the main formulation of the theory are presented subsequently.

In order to establish the transformation-constitutive model, a representative-material sample (constitutive element) with a volume of V, shown in Figure 8, is taken from a bulk single crystal. The temperature (T) is uniformly distributed throughout in the element, and the external macroscopic stress ($\mathbf{\Sigma}$) or strain ($\mathbf{E}$) is applied at the boundary. With the change of temperature, stress, or strain, the transformation and/or variant reorientation may occur. Some kinds of martensitic variants with different orientations will emerge in the element during transformation, and some differently oriented martensitic variants will coalesce when reorientation occurs. Due to the incompatibility of the transformation strain of the variants with the surrounding elastic parent matrix, internal stress will be aroused and elastic-strain energy will be stored in a constitutive element. Many investigators (for example, Wayman[2] and Olson and Cohen[41]) showed that this kind of elastic-strain energy plays a very important role in the thermodynamics and kinetics of thermoelastic martensitic transformation. For example, the stored elastic energy usually opposes the forward transformation and assists the reverse transformation (as the driving force). In the proposed model, in order to analyze the elastic-strain energy in the constitutive element, a concept of inclusion was used. Inclusions are defined as the very small transformed martensite variants. Many micrographs show that a martensite variant appears in the shape of a plate or blade, so the geometric shape of a variant inclusion may be approximated as an oblate spheroid. We further assume that that the short axis of the spherical inclusion is normal to the invariant plane of the variant. So, different kinds of

Table II. The Angles between the Intersection Lines of 24 Invariant Planes on the Surface of the Specimen and the Loading Direction

Variant Number	Angles for Specimen S1 (Degree) Calculated	Angles for Specimen S1 (Degree) Observed	Angles for Specimen S2 (Degree) Calculated	Angles for Specimen S2 (Degree) Observed	Angles for Specimen S3 (Degree) Calculated	Angles for Specimen S3 (Degree) Observed
1	104.536	—	330.065	—	315.452	—
2	30.897	—	187.190	—	136.349	—
3	108.411	—	323.109	—	307.090	—
4	33.395	—	193.594	—	144.507	—
5	107.360	—	332.654	—	315.749	—
6	26.582	—	185.167	—	136.060	—
7	111.223	—	325.922	—	307.899	—
8	28.770	—	191.380	—	143.740	—
9	48.772	—	83.166	—	42.205	—
10	44.238	—	98.340	—	51.292	51.6
11	114.664	—	261.105	—	229.151	—
12	110.784	—	254.846	—	221.417	—
13	93.112	93.90	31.092	—	358.901	—
14	347.693	—	130.572	—	93.006	—
15	162.204	—	308.638	—	272.644	—
16	280.133	—	212.498	—	179.170	—
17	46.265	—	82.465	—	42.426	—
18	41.714	—	95.681	—	50.869	—
19	119.119	—	261.343	—	229.022	—
20	115.544	—	255.247	—	221.696	—
21	82.585	—	34.881	—	2.545	—
22	348.718	—	127.030	—	89.372	—
23	163.205	—	305.159	—	269.027	—
24	266.000	—	216.171	215.2	182.791	—

variants are represented by inclusions with different orientations of the short axes. A constitutive element is composed of the parent phase and a large number of inclusions, and the inclusions are considered to be located stochastically, as the external stress or strain is homogeneous. Therefore, forward transformation is simply the process on which the number of inclusions (N), or the total volume fraction of various kinds of inclusions, increases continuously. Reverse

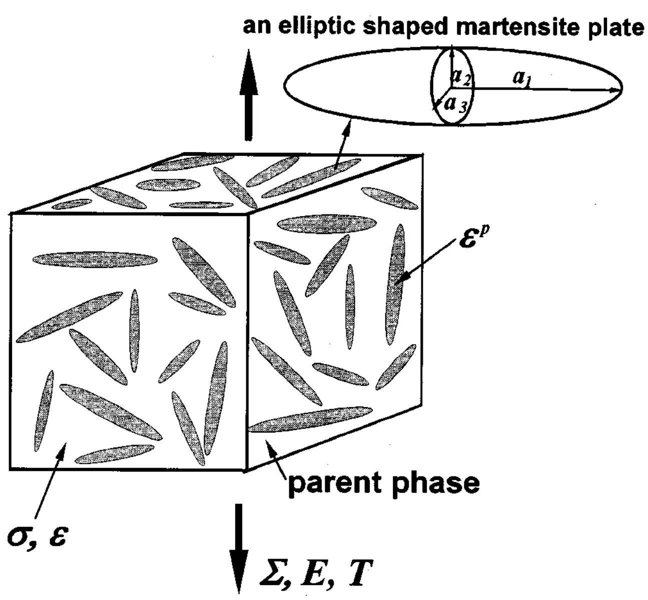

Fig. 8—Illustration of a constitutive element with elliptic-shaped martensite leaves.

transformation is the process in which the number of inclusions decreases, and reorientation is the process in which there is a change of volume fraction between different kinds of variants. We denote the volume occupied by the sth kind of variant ($s = 1, \ldots, N$) by V_s and the corresponding volume fraction by f_s ($= V_s/V$). The total volume of transformed variants (V_i), total volume fraction (f), and the volume of the parent phase (V_p) are

$$V_i = \sum_{s=1}^{N} V_s \; f = \sum_{s=1}^{N} f_s \; V_p = V - V_i \qquad [8]$$

Under the applied global macroscopic stress and temperature, the microscopic stress and strain in the element are expressed by $\boldsymbol{\sigma}$ and $\boldsymbol{\varepsilon}$, respectively. Then, there exists the relation between $\boldsymbol{\sigma}$ and $\boldsymbol{\Sigma}$,

$$\boldsymbol{\Sigma} = \langle \boldsymbol{\sigma} \rangle_V = \frac{1}{V} \int \boldsymbol{\sigma} dV = \sum_{s=1}^{N} f_s \langle \boldsymbol{\sigma} \rangle_{V_s}, + (1 - f) \langle \boldsymbol{\sigma} \rangle_{V_p} \qquad [9]$$

where $\langle \; \rangle$ denotes the volume average over the volume indicated by the subscript. The microscopic and macroscopic strains are assumed to be small and can, therefore, be decomposed into elastic and plastic parts:

$$\mathbf{E} = \langle \boldsymbol{\varepsilon}^e \rangle_V + \langle \boldsymbol{\varepsilon}^p \rangle_V = \mathbf{E}^e + \mathbf{E}^p = \mathbf{M}: \boldsymbol{\Sigma} + \mathbf{E}^p \qquad [10]$$

where $\mathbf{M}$ is the elastic compliance tensor. According to the crystallographic theory of martensitic transformation, we have

$$\mathbf{E}^p = \sum_{s=1}^{N} f_s \boldsymbol{\varepsilon}_s^p = g \sum_{s=1}^{N} f_s \mathbf{R}_s \qquad [11]$$

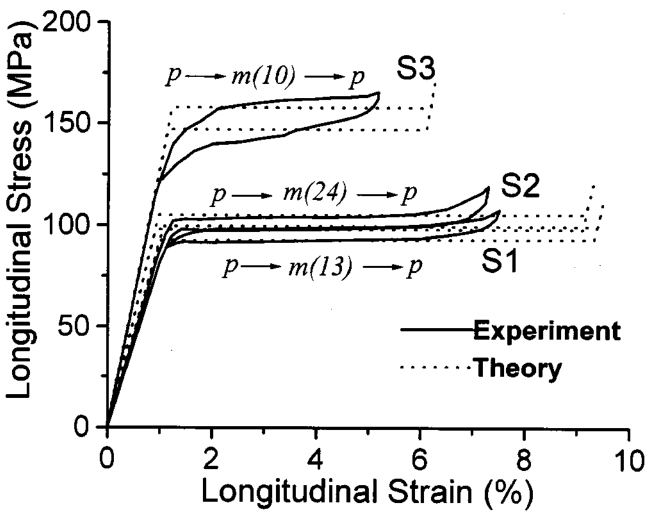

Fig. 9—Comparison of the calculated stress-strain curves and measured stress-strain curves.

By using Mori–Tanaka mean-field theory,[42] the elastic-strain energy induced by internal stress in a unit volume of the element and the total elastic-strain energy (W) per unit volume of the constitutive element can be calculated, respectively.[43] According to the thermodynamics and the internal-variable theory,[44] the constitutive relation can be expressed by

$$\dot{\mathbf{E}} = \mathbf{M}:\dot{\mathbf{\Sigma}} + \sum_{s=1}^{N} \frac{\partial \mathbf{E}_s}{\partial \mathbf{\Sigma}} \dot{f}_s = \mathbf{M}:\dot{\mathbf{\Sigma}} + \sum_{s=1}^{N} \boldsymbol{\varepsilon}_s^p \dot{f}_s \quad (s = 1, \ldots, N) \qquad [12]$$

where

$$\dot{f}_s = \dot{f}_{s0} + \dot{f}_{s1} + \ldots + \dot{f}_{s(s-1)} + \dot{f}_{s(s+1)} + \ldots + \dot{f}_{sN} \quad (s = 1, \ldots, N) \qquad [13]$$

Now we turn to the calculation of the overall stress-strain curve by use of the previous theory. All the material parameters are deduced from relevant test results: the four transformation temperatures, $M_s = -20$ °C, $M_f = -49$ °C, $A_s = -19$ °C, $A_f = 0$ °C, and $M_s = -20$ °C; the equilibrium temperature of the two phases, $T_0 = (M_s + A_s)/2 = -19.5$ °C; a positive constant for the chemical free energy, $k = 0.23$ MPa/°C, from Reference 29; and the elastic compliance constants, $M_{1111} = 4.49 \times 10^{-5}$/MPa, $M_{1122} = -2.12 \times 10^{-5}$/MPa, and $M_{1212} = 0.51 \times 10^{-5}$/MPa. Because the martensite appears in the shape of bands or thin plates, the shape of transformed inclusions is assumed to be flat ellipsoid with the shape parameter $\rho = a_3/a_1 = 0$. Yan *et al.*[22,23,24] have proved that the area encircled by the hysteresis loop (A_h) of the pseudoelastic stress-strain curve, as shown in Figure 3, is exactly equal to the total energy dissipation during the forward and reverse transformation. That is, $A_h = 2D^{tr}$, where D^{tr} is the generalized frictional resistance to either $p \rightarrow m$ or $m \rightarrow p$ interface motion and is assumed to be a material constant. After measuring the areas encircled by the pseudoelastic stress-strain curves of specimens S1, S2, and S3, as shown in Figure 9, we found that the three areas are essentially the same. The difference between the areas of the three curves is less than 5 pct, although the shapes of the three stress-strain hysteresis loops are quite different. Therefore, in our calculation, we resume a mean value of $D^{tr} = 0.28$ MPa.

In light of the directions of the process and the change in material microstructures, thermoelastic martensitic transformation can be divided into three kinds:[4] the forward transformation ($p \rightarrow m$, *i.e.*, the transformation from parent phase to martensite), the reverse transformation ($m \rightarrow p$, *i.e.*, the transformation from martensite to parent phase), and the reorientation ($m \rightarrow m$) between different kinds of martensite habit-plane variants. As observed from the experiments, only one variant appears during the stress-induced transformation under uniaxial loading at a temperature above A_f. Therefore, the forward transformation ($p \rightarrow m$) occurs upon loading, the reverse transformation ($m \rightarrow p$) occurs upon unloading, and the reorientation ($m \rightarrow m$) process under uniaxial loading does not exist. The theoretical result predicts that variant No. 13, for specimen S1, appears upon loading, that is, $p \rightarrow m(13)$, and variant No. 13 disappears upon loading $m(13) \rightarrow p$, which is in complete agreement with the observed result listed in Table II. Similarly, the theory also predicts that variant No. 24, for specimen S2, and variant No. 10, for specimen S3, appear during the transformation, exactly fitting the experimental findings given in Table II. Therefore, the constitutive model predicts that the forward processes and reverse transformation for specimens S1, S2, and S3 are $p \rightarrow m(13) \rightarrow p$, $p \rightarrow m(24) \rightarrow p$, and $p \rightarrow m(10) \rightarrow p$, respectively. This agrees with the observed processes presented in the previous section. Figure 9 shows the comparison between the theoretical stress-strain curves (dotted line) and the measured stress-strain curves (solid line) for the three groups of differently oriented specimens. It can be seen from Figure 9 that the constitutive theory proposed by Yan *et al.* can well predict the transformation stress. It is obvious that the stress-strain curves are orientation dependent and that the dependence of transformation stress levels upon the tensile-axis orientation leads to the difference of pseudoelastic hysteresis. Finally, the measured stress-strain curves in Figure 9 reveal that the transformation hardening is orientation dependent as well. For instance, there is no plateau region in the stress-strain curve of specimen S3, in which the stress increases with a strain increase. On the other hand, Figure 9 indicates that the theory cannot describe the transformation hardening, since the model ignores the surface-energy change.[26] Nevertheless, the proposed constitutive model cannot only predict the forward and reverse transformation precisely, but can also characterize the stress-strain hysteresis behavior during the pseudoelastic deformation under uniaxial tension loading.

VI. CONCLUSIONS

It is found that the stress-strain curves show clear pseudoelastic hysteresis, during which the material undergoes the austenite (DO_3, β_1 phase) to martensite (18R, β_1' phase) stress-induced martensitic transformation. The utilization of a long-focus microscope enabled us to record *in situ* the morphological changes at any stress-strain state during the loading and unloading cycles. It is found that martensite appears in the shape of bands or thin plates on the surface of the specimen. The martensite bands are distributed uniformly and are parallel to each other, which means that only one variant appears. It is found in the experiment that the appearance of martensite is a very quick process and that martensite always jumps out until the specimen is transformed, essentially, to a single crystal. From the computer-recorded micrographs, the angle between the martensite plates and the loading direction can be precisely measured, which agrees well with predictions made by the proposed theory. Under uniaxial tensile loading, the forward transformation ($p \rightarrow m$) occurs upon loading, the reverse transformation ($m \rightarrow p$) occurs upon unloading, and a reorientation ($m \rightarrow m$) process does not exist. The stress-strain curves are significantly orientation dependent. The comparison of the theory to experiments shows that the constitutive model cannot describe the transformation hardening, since the model ignores the surface-energy change. Nevertheless, the proposed constitutive model cannot only predict the forward and reverse transformation, but can also characterize the stress-strain hysteresis behavior during the pseudoelastic deformation under uniaxial tension loading.

ACKNOWLEDGMENTS

Support from the National Natural Science Foundation of China under NNSFC Grant No. 19672026 and from the State Education Commission of China under Grant No. 9400365 is gratefully acknowledged. The Japan Society for the Promotion of Science (JSPS ID No. S-97341) and Professor T. Inoue are acknowledged for support to KCH. The authors also thank the technical assistance from Messrs. Xin Hua and G. Xu and Ms. T. Xu.

REFERENCES

1. M.S. Wechsler, D.S. Lieberman, and T.A. Read: *Trans. AIME*, 1953, vol. 197, pp. 1503-15.
2. C.M. Wayman: *Introduction to the Crystallography of Martensite Transformation*, The MacMillan Co., New York, NY, 1964.
3. J.S. Bowles and J.K. Mackenzie: *Acta Metall.*, 1954, vol. 2, pp. 129-37.
4. L. Delaey, R.V. Krishnan, H. Tas, and H. Warlimont: *J. Mater. Sci.*, 1974, vol. 9, pp. 1521-55.
5. J.W. Christian: *Metall. Trans. A*, 1982, vol. 13A, pp. 509-38.
6. R.D. James: *J. Mech. Phys. Solids*, 1986, vol. 34, pp. 359-94.
7. J.M. Ball and R. D. James: *Arch. Rat. Mech. Anal.*, 1987, vol. 100, pp. 13-52.
8. K. Bhattacharya: *Acta Metall.*, 1991, vol. 39, pp. 2431-44.
9. R. Abeyaratne and J.K. Knowles: *J. Mech. Phys. Solids*, 1993, vol. 41, pp. 541-71.
10. R., Abeyaratne, C. Chu, and R.D. James: *ASME Appl. Mech. Div.*, 1994, vol. 189, pp. 85-98.
11. F. Falk: *Acta Metall.*, 1980, vol. 28, pp. 1773-80.
12. E. Patoor, T.A. Eberhard, and M. Berveiller: *Arch. Mech.*, 1988, vol. 40, pp. 775-94.
13. I. Muller and H. Xu: *Acta Metall.*, 1991, vol. 39, pp. 263-71.
14. C. Chu and R.D. James: *ASME Appl. Mech. Div.*, 1993, vol. 181, pp. 61-69.
15. K. Tanaka, E.R. Oberaigner, and F.D. Fischer: in *Mechanics of Phase Transformations and Shape Memory Alloys*, L.C. Brinson and B. Moran, ed., ASME, Fairfield, NJ, 1994, AMD-vol. 189/PVP-vol. 292, pp. 151-57.
16. K. Tanaka, F. Nishimura, F.D. Fischer, and E.R. Oberaigner: *Proc. MECAMAT 95*, C. Lexcellent, E. Patoor, and E. Gautier, eds., *J. Phys. Coll. 1, Suppl. J. Phys. III*, Les Editions De Physique, Les Ulis, 1996, vol. 6 C1-455/C1-463.
17. C. Liang and C.A. Rogers: *J. Eng. Math.*, 1992, vol. 26, pp. 429-43.
18. Q.P. Sun and K.C. Hwang: *J. Mech. Phys. Solids*, 1993, vol. 41, pp. 1-33.
19. Q.P. Sun and K.C. Hwang: *Adv. Appl. Mech.*, 1994, vol. 31, pp. 249-98.
20. F.D. Fischer, Q.P. Sun, and K. Tanaka: *ASME Appl. Mech. Rev.*, 1996, vol. 49, pp. 317-64.
21. F.D. Fischer, E.R. Oberaigner, K. Tanaka, and F. NishimuraI: *Int. J. Solids Struct.*, 1998, vol. 35, pp. 2209-27.
22. W. Yan, Q.P. Sun, and K.C. Hwang: *Proc. 3rd Asia–Pacific Symp. on Advances in Engineering Plasticity and Its Application*, 21–24 August, 1996, Hiroshima, Japan, T. Abe and T. Tsuta eds., Pergamon, Amsterdam-Oxford-New York-Tokyo, pp. 9-14.
23. W. Yan, Q.P. Sun, and K.C. Hwang: *Int. J. Plasticity*, 1997, vol. 13, pp. 201-13.
24. W. Yan, Q.P. Sun, and K.C. Hwang: *Sci. China*, 1998, vol. A28, pp. 275-82.
25. X. Chen, D.N. Fang, and K.C. Hwang: *Acta Material.*, 1997, vol. 45, pp. 3181-89.
26. G.Q. Song, Q.P. Sun, and K.C. Hwang: *IUTAM Symp. on Variations of Domains and Free Boundary Problems*, P. Argoul, M. Fremond, and Q.S. Nguyen, eds., 22–25 April, 1997, Paris, France, Kluwer Academic Publishers, Dordrecht, The Netherlands, 1999, pp. 25-34.
27. Z.K. Lu and G.J. Weng: *J. Mech. Phys. Solid*, 1997, vol. 45, pp. 1905-28.
28. K. Okamoto, S. Ichinose, K. Morii, K. Otsuka, and K. Shimizu: *Acta Metall.*, 1986, vol. 34, pp. 2065-73.
29. H. Horikawa, S. Ichinose, K. Morii, S. Miyazaki, and K. Otsuka: *Metall. Trans. A*, 1988, vol. 19A, pp. 915-23.
30. T.W. Shield: *J. Mech. Phys. Solids*, 1995, vol. 43, pp. 869-95.
31. E.S. Machlin and S. Wenig: *Acta Metall.*, 1953, vol. 1, pp. 480-89.
32. R.V. Krishnan and C. Brown: *Metall. Trans.*, 1973, vol. 4, pp. 423-29.
33. S. Ichinose, Y. Funatsu, and K. Otsuka: *Acta Metall.*, 1985, vol. 33, pp. 1613-25.
34. M. Suezawa and K. Sumino: *Scripta Metall.*, 1976, vol. 10, pp. 789-96.
35. G.V. Kurdjumov and L.G. Khandros: *Dokl. Akad. Nauk SSSR*, 1949, vol. 66, pp. 211-24.
36. M.J. Duggin and W.A. Rachinger: *Acta Metall.*, 1964, vol. 12, pp. 529-38.
37. K. Otsuka, C.M. Wayman, K. Nakai, H. Sakamoto, and K. Shimizu: *Acta Metall.*, 1976, vol. 24, pp. 207-18.
38. K. Oishi and C. Brown: *Metall. Trans.*, 1971, vol. 2, pp. 1971-77.
39. K. Otsuka and K. Shimizu: *Trans. JIM*, 1974, vol. 15, pp. 201-10.
40. H.B. Xu, S.L. Fu, and S.S. Tan: *Z. Metallkd.*, 1993, vol. 84, pp. 469-77.
41. G.B. Olson and M. Cohen: *Metall. Trans. A*, 1976, vol. 7A, pp. 1897-1904.
42. T. Mori and K. Tanaka: *Acta Metall.*, 1973, vol. 21, pp. 571-74.
43. T. Mura: *Micromechanics of Defects in Solid*, Martinus Nijhoff, Dordrecht, 1987.
44. J.R. Rice: *J. Mech. Phys. Solids*, 1971, vol. 19, pp. 433-55.